Photoinduced Dynamics of TiO_2 Doped with Cr and Sb

Toshitatsu Ikeda,[†] Tomonori Nomoto,[†,‡] Kazuo Eda,[†] Yasuhisa Mizutani,[§] Hideki Kato,[||] Akihiko Kudo,[‡,||] and Hiroshi Onishi*[,†]

Department of Chemistry, Kobe University, Rokkodai, Nada, Kobe 657-8501, Japan, Molecular Photoscience Research Center, Kobe University, Rokkodai, Nada, Kobe 657-8501, Japan, Department of Chemistry, Tokyo University of Science, Kagurazaka, Shinjuku, Tokyo 162-8601, Japan, and Core Research for Evolutional Science and Technology, Japan Science and Technology Agency, Honcho, Kawaguchi, Saitama 332-0012, Japan

Received: July 5, 2007; In Final Form: October 28, 2007

Rutile particles doped by Cr and Sb with Sb/Cr ratios greater than unity were active for photocatalytic O_2 evolution from an aqueous silver nitrate solution under visible light irradiation. Two vibrational bands appeared in Raman scattering resonant to the electronic absorption and were assigned to symmetric breathing modes of the CrO_6 octahedron and neighboring TiO_6 octahedra, on the assumption that Cr dopant atoms exactly replaced Ti cations in rutile. Electrons excited with 355-nm and 532-nm light pulses showed absorption of mid-IR light, which was traced as a function of the time delay in a microsecond domain. By optimizing the Sb/Cr ratio, electron−hole recombination was retarded compared with that in non-doped rutile. Chromium dopants when accompanied with antimony dopants are proposed to trap the charge carriers without much enhancement of the recombination. The optimized Sb/Cr ratios were common for both the visible light-induced O_2 production and the retarded recombination, suggesting that the charge carriers of the retarded recombination are used to produce O_2.

1. Introduction

The photocatalytic water splitting reaction provides a large amount of hydrogen fuel free from CO_2 release when driven by solar light. A number of inorganic compounds synthesized thus far exhibit high activity in ultraviolet (UV) light irradiation.[1−4] Intense efforts are currently being made to develop catalysts for efficient H_2 production with visible light. Although the stoichiometric production of H_2 and O_2 has been demonstrated,[5−8] more efficient catalysts are required to make the process practical.

Foreign-element doping provides a donor or acceptor level in the band gap to sensitize a UV-driven catalyst to visible light. For example, TiO_2 absorbs visible light when doped with transition metals.[9] Trivalent chromium cation dopant has been examined along this scheme of sensitization.[9−12] However, the photocatalytic production of H_2 and O_2 has not yet been achieved with Cr-doped TiO_2. Chromium cations in the 6+ state and oxygen anion vacancies are usually produced in the doped TiO_2 to maintain the balance of the positive and negative ionic charges. Photoexcited electrons and holes efficiently recombine at these impurities and defects.

Two of the present authors[13] recently reported photocatalytic O_2 production from an aqueous $AgNO_3$ solution over rutile TiO_2 doped with Cr *and* Sb under visible light irradiation. The atom number ratio, Sb/Cr, should be greater than unity to activate the visible light-induced O_2 production. The ionic state of Sb is 5+ in the doped catalysts. Neither Cr^{6+} nor oxygen vacancy is required to stabilize Cr^{3+} in the presence of an equivalent amount of Sb^{5+}. This concept of cation charge compensation may be applied to sensitize wide band gap photocatalysts for water splitting and also degradation of organic compounds. The proposed scheme of photoexcitation is illustrated in Figure 1. Electrons in the occupied orbitals of Cr^{3+} are excited to the conduction band of TiO_2 by absorbing visible light.

In previous work, we proposed the ability of time-resolved infrared (IR) absorption to observe photoexcited electron dynamics.[14,15] Mid-IR light is absorbed by electrons in the conduction band or energetically shallow trap states.[16−18] Studies of electron dynamics for different TiO_2 catalysts[17,19] including P25,[20,21] sulfur-doped TiO_2,[22] and dye-sensitized TiO_2[23] have been conducted, and infrared-based detection of electrons is possible on catalysts other than TiO_2, as evidenced with $K_3Ta_3B_2O_{12}$[24] and La-doped $NaTaO_3$.[25] In the present study, TiO_2 doped with Cr and Sb is characterized by IR absorption and Raman spectroscopy, with particular interest paid to the dynamics of the excited electrons.

2. Experimental Section

Chromium and antimony were doped to rutile TiO_2 particles by calcining mixtures of rutile, Cr_2O_3, and Sb_2O_3 at 1420 K for 10 h in air.[13] The amount of Cr atoms in the starting materials was fixed at 2.3 mol % relative to Ti atoms. The Sb/Cr atom ratio was tuned to 0, 0.5, 1.0, 1.5, 2.5, and 3.5. TiO_2 doped with 3.45 mol % Sb alone was prepared for comparison. Each of the calcined catalysts (0.3 g) was irradiated with a filtered 300 W Xe lamp (Perkin-Elmer, CERMAX PE-300BF) in an aqueous $AgNO_3$ solution (0.05 mol L^{-1}). The incident light wavelength was 420 nm or longer. The rate of O_2 production was determined using a gas chromatograph.

The UV−visible absorption of the catalyst powder was observed by a spectrometer (JASCO, V-570) equipped with an

* To whom correspondence should be addressed. E-mail: oni@kobe-u.ac.jp.
[†] Department of Chemistry, Kobe University.
[‡] Japan Science and Technology Agency.
[§] Molecular Photoscience Research Center, Kobe University.
[||] Tokyo University of Science.

10.1021/jp0752264 CCC: $40.75
Published on Web 01/09/2008

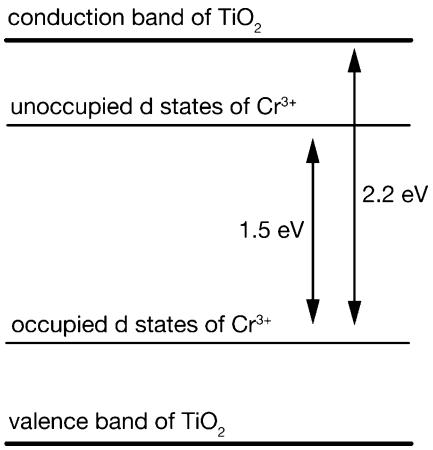

Figure 1. Proposed electronic states of TiO_2 doped with chromium and antimony.

integration sphere. The size, shape, and Sb content of the calcined catalyst particles were determined using scanning electron microscopes (JEOL, JSM-5610LVS and JSM-6700F) with an energy dispersive X-ray spectrometer (EDS). The calcined catalysts were fixed on a CaF_2 plate and placed in a gas cell for IR and Raman studies. Steady-state IR absorption was observed with an FT-IR spectrometer (JASCO, FT/IR 610) at a resolution of 4 cm^{-1}. The steady-state Raman spectrum was observed with two excitation wavelengths. To be resonant to the visible light absorption of the doped catalysts, a He−Cd laser source (Kinmon, IK4401R-D) was used to prepare 442 nm wavelength CW light of 35 mW. Raman scattered light was collected at 135° by a pair of fused quartz lenses, f-matched to a 65 cm spectrograph (Spex, Triplemate 1877) equipped with a holographic grating (2400 grooves mm^{-1}) and a liquid-nitrogen-cooled CCD detector (Princeton Instruments, LN/CCD 1100PB). To be out of resonance, a FT-Raman spectrometer (Perkin-Elmer, System2000) was used with excitation wavelength of 1064 nm. In the time-resolved IR absorption study, a Q-switched Nd:YAG laser source (LOTIS, LS-2139) was operated at 100 Hz repetition rate. The fundamental output of 10 ns time width was frequency doubled (tripled) to produce pump pulses of 532 (355) nm wavelength. The catalyst on the plate was irradiated with pump pulses of 1.3 mJ. The diameter of the pump beam was 6 mm. Continuous-wave IR light from a ceramic source was focused on the catalyst, and the transmitted portion was dispersed with a grating monochromator with a focal length of 25 cm (JASCO, CT25). An MCT detector received the monochromatized light. The MCT signal voltage was amplified with an AC-coupled amplifier (NF circuit, NF 5307 or Stanford Research System, SR560). By accumulating 4000 responses, an absorbance change as small as 10^{-6} was traced as a function of the time delay from the pump pulse. The cell was filled with argon gas of 10 Torr to minimize the temperature jump of the catalyst caused by pump irradiation. Thermal emission of IR light was observed when irradiated in a vacuum.

3. Results and Discussion

3.1. Electronic States of the Sensitized Catalysts. Figure 2 shows the diffuse reflectance spectra of non-doped TiO_2 (TiO_2), Sb-doped TiO_2 (TiO_2:Sb), Cr-doped TiO_2 (TiO_2:Cr), and Cr-and-Sb-doped TiO_2 (TiO_2:Sb/Cr = 0.5, 1.0, 1.5, 2.0, 2.5 and 3.5) catalysts. TiO_2 and TiO_2:Sb were transparent to visible light of 420 nm or longer wavelengths. TiO_2:Sb contains Sb^{3+} and Sb^{5+} dopant atoms according to our XPS study.[13] For TiO_2:Sb/Cr catalysts with Sb/Cr ≥ 1.0, two absorption bands were

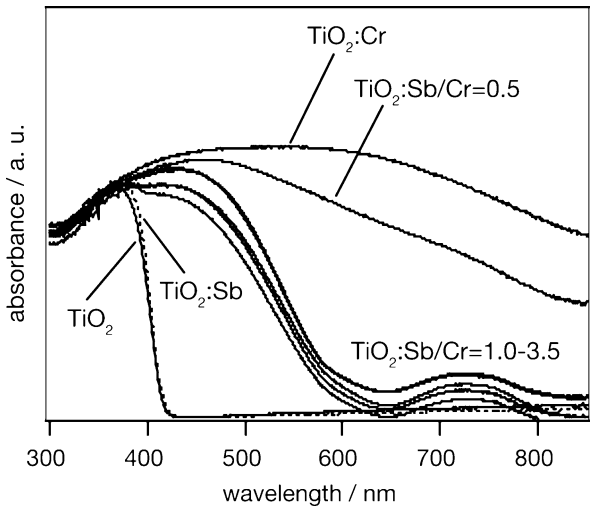

Figure 2. Diffuse reflection spectra of the catalysts. Spectra of TiO_2, TiO_2:Cr, TiO_2:Sb/Cr = 0.5, 1.0, 1.5, 2.0, 2.5, and 3.5 are shown with solid lines. Spectrum of TiO_2:Sb is shown with a broken line.

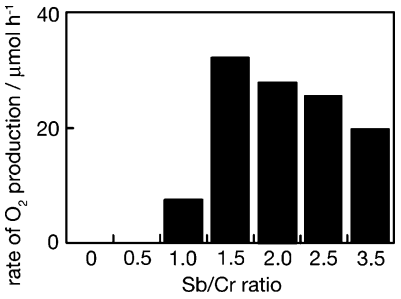

Figure 3. Rate of O_2 production on TiO_2:Sb/Cr with different Sb/Cr ratios.

identified; a major band centered at 500 nm and a minor band centered at 730 nm. These features reproduced our previous results. By adding an equivalent amount of Sb, the oxidation state of Cr dopants is controlled to be trivalent. When an equivalent number of Cr and Sb are doped, the two dopants are expected to be Cr^{3+} and Sb^{5+}. Excess Sb dopants, if any, disproportionate to Sb^{3+} and Sb^{5+} as in TiO_2:Sb. The major absorption band arises from the transition from the occupied d-states of Cr^{3+} to the conduction band of TiO_2 as illustrated in Figure 1. The d−d transition of the Cr^{3+} dopants presents the minor absorption band.[12]

TiO_2:Cr and TiO_2:Sb/Cr = 0.5 exhibited absorption over the entire wavelength range examined. The oxidation state of Cr was heterogeneous in the absence of Sb codopant. Oxygen vacancies should have been created to maintain charge neutrality. Electronic transitions at these undesired sites gave the broad absorption band.

3.2. Photocatalytic O_2 Production. The rate of O_2 production driven by the visible light, the wavelength of which was longer than 420 nm, is shown in Figure 3. On TiO_2:Cr and TiO_2:Sb/Cr = 0.5, no oxygen was produced. A finite amount of O_2 appeared on TiO_2:Sb/Cr =1.0. A sharp increase in O_2 production for TiO_2:Sb/Cr = 1.0 and 1.5 was followed by a gradual decrease for TiO_2:Sb/Cr = 2.0−3.5. The photocatalytic activity and Sb/Cr-ratio dependence of the current set of catalysts reproduced our previous results.[13] TiO_2:Sb/Cr = 1.0 was less active than TiO_2:Sb/Cr = 1.5, probably because the Sb/Cr ratio shifted from unity and the ionic charge of the two dopants was only partially compensated. Some antimony in the starting material could be lost in the high-temperature calcination,

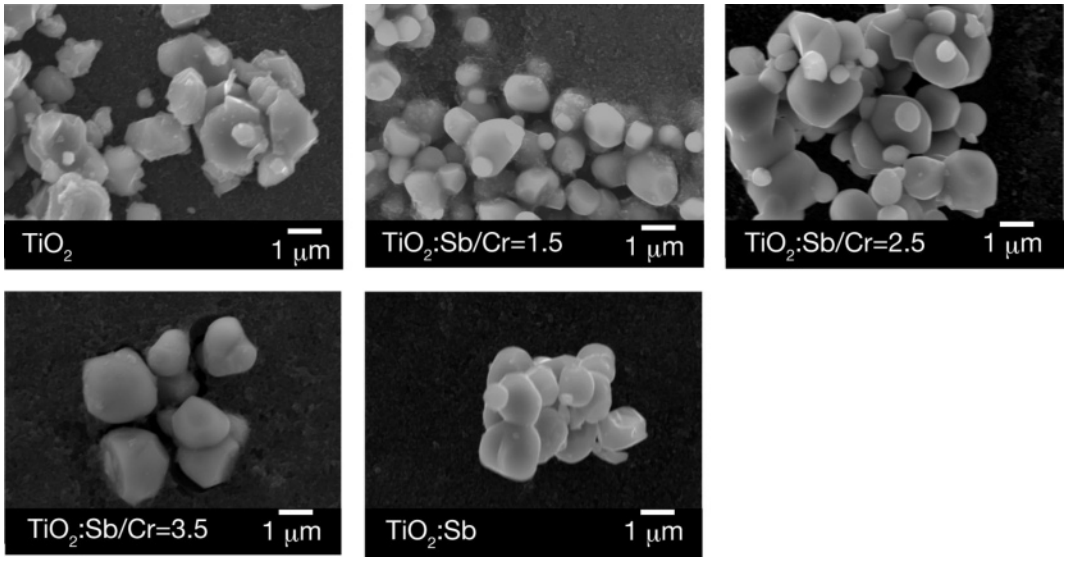

Figure 4. Scanning electron micrographs of TiO_2, TiO_2:Sb, TiO_2:Sb/Cr = 1.5, 2.5, and 3.5 catalysts.

suggesting a small amount of excess Cr poisons the photocatalytic reaction.

Alternatively, the O_2 production rate was scarcely affected by Sb/Cr ratios over 1.5. Excess Sb dopants can be autocompensated by creating an equivalent amount of Sb^{3+} and Sb^{5+}.[13] Vaporization of excess Sb is another possible reason for the O_2 production insensitive to Sb/Cr. When TiO_2 doped with 10 and 30 mol % Sb alone was calcined, 3.6 and 4.5 atom% Sb was detected by EDS. Figure 4 shows scanning electron micrographs of TiO_2, TiO_2:Sb, TiO_2:Sb/Cr = 1.0, 2.0, and 3.5. The size of catalyst particles was in the range of 1−2 μm.

3.3. Raman Scattering Resonant to the Electronic Excitation. Dopant atoms affect vibrations of the TiO_2 lattice. Raman scattering resonant to the dopant-induced absorption provides the frequency of affected vibrations. Figure 5a shows the Raman spectra of nine catalysts excited with 442-nm light. Two major bands appeared for the non-doped TiO_2 at 610 and 440 cm^{-1} and were assigned to rutile lattice vibrations in A_{1g} and E_g symmetry. The rutile lattice of the *P*4/*mnm* space group possesses four Raman-active modes at 830 (B_{2g}), 610 (A_{1g}), 450 (E_g), and 140 (B_{1g}) cm^{-1}.[26] On the visible light-sensitized catalysts, two small bands were additionally identified at 810 and 700 cm^{-1}. The intensity of these additional bands was sensitive to the dopant concentrations. For Cr-containing catalysts, these bands strengthened with increasing Sb/Cr ratio to saturate at Sb/Cr = 1.5 and above. This positive relation with the Sb/Cr ratio allows us to assign the additional bands to the TiO_2 lattice affected by Cr^{3+} dopants. The fraction of Cr^{3+} over highly oxidized states increased with the Sb/Cr ratio, as evidenced by XPS spectra.[13] It is difficult to assign the additional bands to vibrations of antimony oxide because they were absent for TiO_2:Sb. Sb_2O_3 presents a B_{2g} mode at 712 cm^{-1}, while Sb_2O_4 containing Sb^{3+} and Sb^{5+} presents five Raman bands at 831, 759, 722, 658, and 616 cm^{-1}.[27]

Raman spectra shown in panel b were obtained with excitation by 1064-nm light. The 810 and 700 cm^{-1} bands were absent for the whole set of the catalysts, whereas the major bands appeared at 610 and 440 cm^{-1}. When an electronic transition is resonant to the incident photon energy, the probability of Raman scattering is remarkably enhanced. The electronic transition of the sensitized catalysts is resonant to 442-nm light and non-resonant to 1064-nm light. Hence, vibrational modes localized around visible light-absorbing centers exhibit the two Raman bands at 810 and 700 cm^{-1}.

Let us draw a picture of the visible light-absorption centers on the basis of the Raman band frequencies. TiO_2:Cr contains Cr^{3+} and Cr^{6+}, whereas TiO_2:Sb/Cr includes Cr^{3+} and Sb^{5+}, according to the XPS results.[13] Cr_2O_3 of the corundum structure,[28] Cs_2CrO_4 with CrO_4 tetrahedra,[29] and $Cs_2Cr_2O_7$ with connected tetrahedra[29] have no Raman band in the range of 800−600 cm^{-1}. However, Raman bands of CrO_2, which is of rutile structure, are at 680 (B_{2g}), 570 (A_{1g}), 460 (E_g), and 150 (B_{1g}) cm^{-1}.[30] The frequency of the B_{2g} band is close to 700 cm^{-1}. When a CrO_6 octahedron is substituted for a TiO_6 in rutile, the B_{2g} mode of the CrO_6 may appear at 700 cm^{-1}. The band observed at 700 cm^{-1} is hence assigned to the B_{2g} mode of the CrO_6 octahedron in TiO_2.

The assignment of the 810 cm^{-1} band is not straightforward. CrO_2 has no Raman active mode around 800 cm^{-1}. We propose that the B_{2g} mode of the CrO_6 octahedron couples with the rutile lattice mode of common symmetry, the B_{2g} mode of 830 cm^{-1}. The coupling mixes the characters of the B_{2g} modes of the CrO_6 octahedron and TiO_6 octahedra and gives the resonance Raman intensity to the band that is mainly due to the B_{2g} TiO_6 mode. The Raman band at 810 cm^{-1} can be assigned to the B_{2g} mode of TiO_6 octahedra affected by the neighboring CrO_6 octahedron. This interpretation reasonably explains the appearance of 810 cm^{-1} and 700 cm^{-1} bands in pairs.

The observed comparable intensity of the 810 and 700 cm^{-1} bands suggests efficient coupling of the TiO_6 and CrO_6 modes. When the Cr dopant atom is in an interstitial site, which is inequivalent to Ti sites, the coupling of the vibrational modes cannot be efficient. This consideration strongly suggests that Cr dopant atoms exactly replaced Ti cations in the rutile lattice.

The CrO_6 octahedra of CrO_2 and TiO_6 octahedra of TiO_2 breathe in the B_{2g} mode with the metal−oxygen distances stretched in phase, as illustrated in Figure 6. The 442-nm light causes an electron transition from the occupied state of Cr^{3+} to the conduction band of TiO_2 according to the scheme of Figure 1. The ionic radii of the Cr and Ti cations are accordingly affected to induce the symmetric breathing of octahedra. The Raman scattering due to the symmetric breathing modes is likely to be enhanced by resonance with the electronic transition in a Franck−Condon manner.[31] In fact, the B_{2g} Raman band of non-doped rutile undergoes resonance enhancement with 325-nm excitation,[32] enabling electron transition to the conduction band. To efficiently enhance the symmetric breathing mode of CrO_6, the electronic excited state associated with the resonance

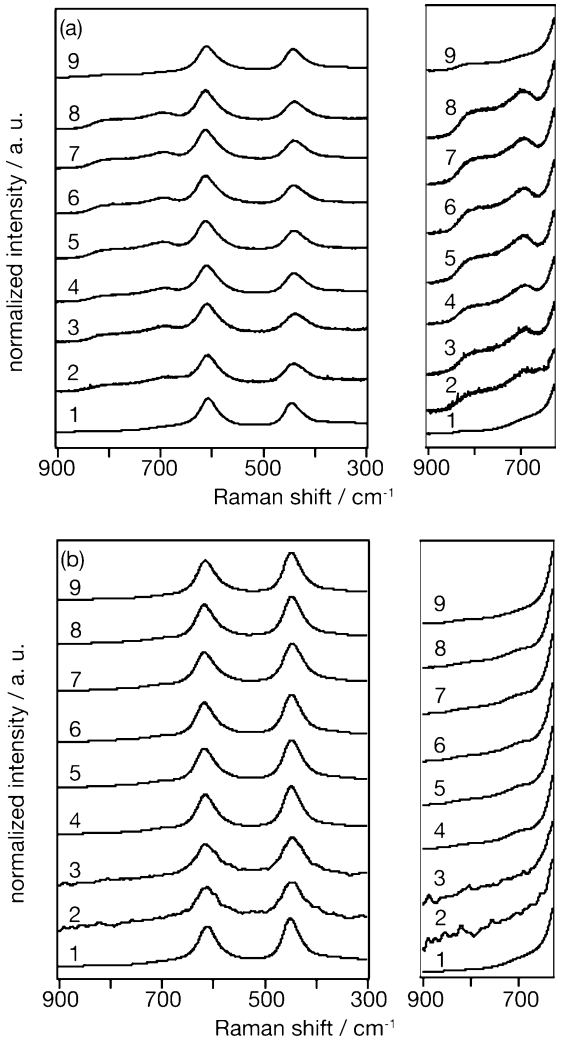

Figure 5. Raman spectra of nine catalysts. Excitation wavelength: (a) 442 nm and (b) 1064 nm. Curves: 1, TiO_2; 2, TiO_2:Cr, 3, TiO_2:Sb/Cr = 0.5; 4, TiO_2:Sb/Cr = 1.0; 5, TiO_2:Sb/Cr = 1.5; 6, TiO_2:Sb/Cr = 2.0; 7, TiO_2:Sb/Cr = 2.5; 8, TiO_2:Sb/Cr = 3.5; 9, TiO_2:Sb. Vertical scale of each spectrum is normalized in terms of 610 cm^{-1} band intensity. Magnifications in the 900−630 cm^{-1} range are presented in the right panels.

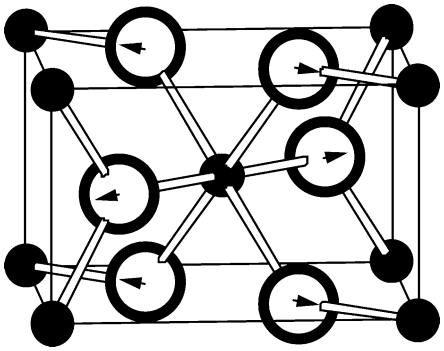

Figure 6. Raman-active B_{2g} mode of lattice vibration in rutile. Metal cations and oxygen anions are represented by dark and white spheres, respectively. Displacements of oxygen anions are shown by arrows.

enhancement should be symmetric around the Cr center. This can be the case when each Cr dopant is surrounded by eight TiO_6 octahedra and the electron transferred from the Cr center is delocalized over eight neighboring Ti cations. This provides negative evidence of paired dopants, such as Cr−O−Sb, embedded in rutile.

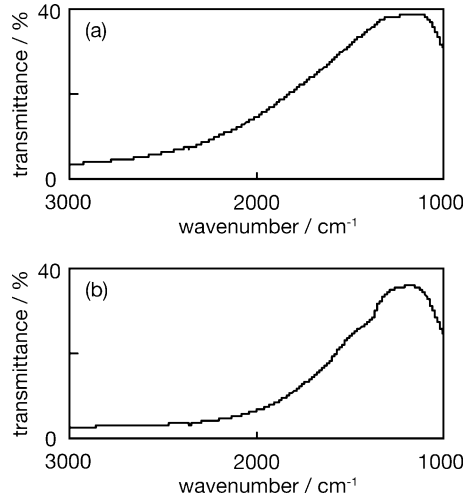

Figure 7. Infrared transmittance spectra of (a) TiO_2 and (b) TiO_2:Sb/Cr = 1.5 observed in the dark.

In the preceding paragraphs, the resonance enhancement of the Raman scattering was assumed to interpret the observed spectra. Another character of Raman scattering resonant to an electronic transition is the restricted depth of sampling. The incident light is absorbed by the material efficiently and cannot penetrate into the bulk. If Cr dopant atoms were segregated to the surface of the catalysts, the additional bands at 810 and 700 cm^{-1} would appear without the resonance enhancement. This was not the case, however. When Cr dopant atoms were segregated to the surface, the other Cr-induced modes should appear in the spectrum. There was no signature of the A_{1g} mode at 570 cm^{-1}. The observed spectra shown in Figure 5a are thus interpreted with the resonance enhancement.

3.4. Steady-State IR Absorption in the Dark. The steady-state IR transmittance spectra of TiO_2 and TiO_2:Sb/Cr = 1.5 are shown in Figure 7. Transmittance monotonously decreased with increasing wavenumber. The low transmission at the high wavenumbers is ascribed to light scattering by micrometer-sized particles. Doping Cr or Sb did not affect the scattering and absorption of IR light. The other doped catalysts presented similar spectra.

3.5. IR Absorption Induced by Electronic Excitation. Transient absorption of IR light was induced by pump light pulses. Panel a of Figure 8 shows the IR absorption spectrum of TiO_2:Sb/Cr = 1.0 caused by the 355-nm irradiation. The transient spectrum at different time delays presented a structureless feature that monotonously increased with decreasing wavenumber. The absolute absorbance reduced with the time delay. The absorption spectra of TiO_2 irradiated with 355-nm pulses, and TiO_2:Sb/Cr = 1.0 irradiated with 532-nm pulses, are shown in panels b and c, respectively. The 532-nm light pulse irradiation was not examined on the undoped catalyst because no absorption was found in its diffuse reflectance spectrum of Figure 2. A 532-nm light irradiation was examined on P25 catalyst and exhibited no response in transient IR absorption.[21]

The spectra shown in a−c resemble each other and were assigned to absorption by photoexcited electrons. Broken lines indicate fitting to $\Delta abs = A\nu^{-6}$ with ν as a wavenumber. Free electrons excited in the conduction band are trapped in mid-gap states within picoseconds.[33] A finite fraction of the trapped electrons are thermally excited to the conduction band. Conduction-band electrons give absorption characterized by a monotonous spectrum formulated by $\nu^{-1.5}$, when the momentum required for the intraband transition is provided by acoustic

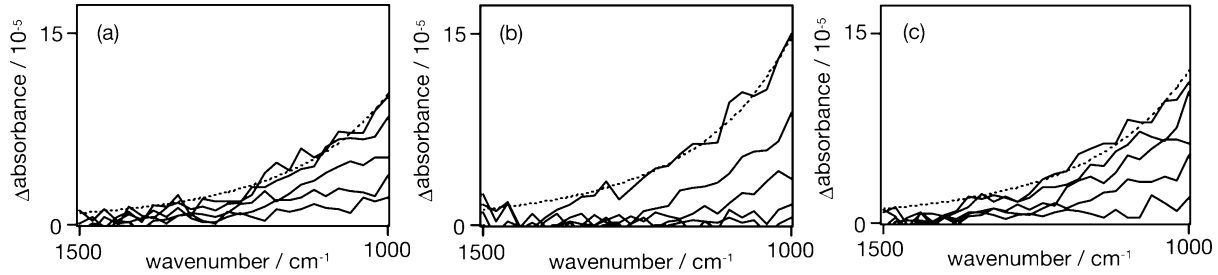

Figure 8. Transient IR absorption spectra of (a) TiO_2:Sb/Cr = 1.0 and (b) TiO_2 induced by 355-nm light pulses. Five spectra were observed at time delays of 0, 0.5, 1, 2, and 5 ms. Broken lines represent fittings to $\Delta abs = A\nu^{-6}$. Spectra in c were observed on TiO_2:Sb/Cr = 1.0 irradiated with 532-nm light pulses.

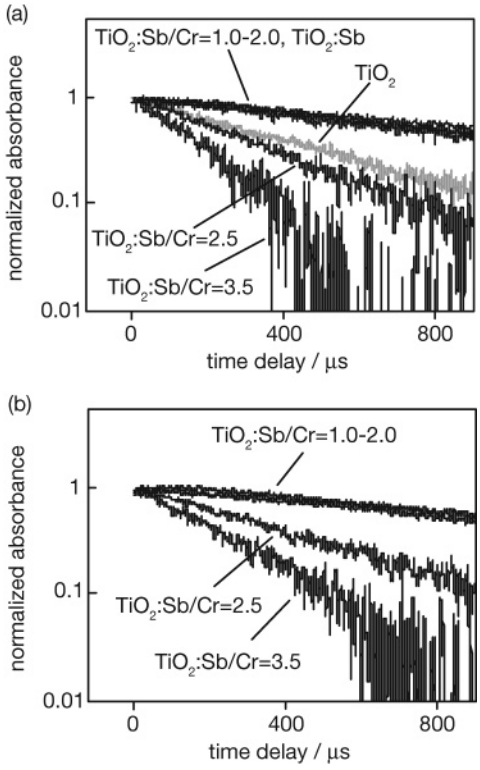

Figure 9. Infrared absorbance at 1100 cm^{-1} as a function of time delay. TiO_2, TiO_2:Sb and TiO_2:Sb/Cr = 1.0−3.5 catalysts were irradiated with (a) 355-nm and (b) 532-nm light pulses.

phonons.[34] Actually, a transient absorption spectrum of $\nu^{-1.5}$ was observed for P25 irradiated with 355-nm pulses.[21] Another mechanism of IR absorption is the optical transition of the trapped electrons to the conduction band. The energy of the absorbed photon is larger than the ionization energy of the traps in this scheme. Although the observed $p = 6$ deviated from the expected numbers, we still assign the monotonous absorption to the excited electrons. Photoexcited ZnO exhibited an absorption spectrum of $\nu^{-4.5}$, and the higher than expected order was ascribed to the non-parabolic band of ZnO.[35] A possible reason for the deviation is scattering of high-wavenumber IR light by our catalysts. Light scattering of catalyst particles dominated the steady-state transmittance spectra (Figure 7). Light scattering ability is enhanced by photoexcited electrons that are more mobile than the ground-state electrons.

3.6. Recombination Dynamics Traced by Transient IR Absorption. Electrons excited by pump light pulses recombined with holes. The number of electrons not yet recombined was traced by the electron-induced monotonous absorption of IR light. Figure 9 shows the absorbance observed at 1100 cm^{-1} as a function of the time delay up to 900 μs. When TiO_2 was irradiated with 355-nm light, the IR absorption appeared and decayed in first-order kinetics with a time constant of 440 μs, as shown in panel a. Because the catalyst was placed in an argon atmosphere, the electron decay is ascribed to recombination in the bulk, not to photocatalytic reactions at the surface.

On TiO_2:Cr and TiO_2:Sb/Cr = 0.5, the transient absorption was not observed. Instead, thermal radiation of IR light was detected when irradiated with the 355-nm light pulses. Electron−hole recombination was completed to convert the incident UV photons into heat within the time resolution of our spectrometer, 50 ns. Centers of efficient recombination are present in the two catalysts doped with excess Cr, and the absence of photocatalytic O_2 production on the two catalysts is consistent with the efficient recombination.

The IR absorption was observed for TiO_2:Sb/Cr = 1.0 and TiO_2:Sb/Cr = 2.0. The efficiency of recombination was reduced by tuning the Sb/Cr ratio. The threshold ratio of IR absorption, Sb/Cr = 1.0, suggests that one Sb atom per Cr is required to suppress the recombination probability. At this threshold ratio, the photocatalytic activity for O_2 production appeared as shown in Figure 3.

Oxygen vacancies and dopants themselves are possible centers of recombination. The oxidation state of the dopants was found to be Cr^{3+} and Sb^{5+} in TiO_2:Sb/Cr = 1.0.[13] There is no need to create oxygen vacancies in TiO_2 when an equivalent number of Cr^{3+} and Sb^{5+} are doped. The two dopant cations are substituted for two Ti^{4+} cations, as evidenced in the resonance Raman results. The sum of cation charges is conserved, and the periodic lattice is maintained. The ionic radii of Cr^{3+} (0.062 nm) and Sb^{5+} (0.060 nm) are close to that of Ti^{4+} (0.061 nm).[36] The rutile lattice of the doped catalysts indeed remained with a shift of X-ray diffraction peaks by 0.1° or less.[13] In the current study, we have proven that electron−hole recombination is scarcely enhanced on Cr^{3+} and Sb^{5+} cations doped in this manner.

The other important feature of electron dynamics is the reduced recombination rate. The time constant of the first-order decay increased from 440 μs for TiO_2 to 1100 μs for TiO_2:Sb/Cr = 1.0. The reduced recombination rate was unexpected. Doping heterogeneous elements enhances the recombination rate in TiO_2-based catalysts, even when the doped materials are sensitized to visible light. This is because dopant atoms always disturb the periodic potential of the TiO_2 lattice. Electrons and holes are trapped and then recombined on the dopants. This accepted scheme of doping is challenged by the current results of Cr^{3+} dopants compensated with Sb^{5+}. The compensated dopants affect the periodic potential of the lattice only to trap electrons and holes, while the recombination is scarcely catalyzed. This trap and release process makes the charge carriers less mobile, thereby reducing the recombination rate.

The recombination kinetics of TiO_2:Sb/Cr = 2.0 and TiO_2:Sb reproduced those of TiO_2:Sb/Cr = 1.0. The excess Sb

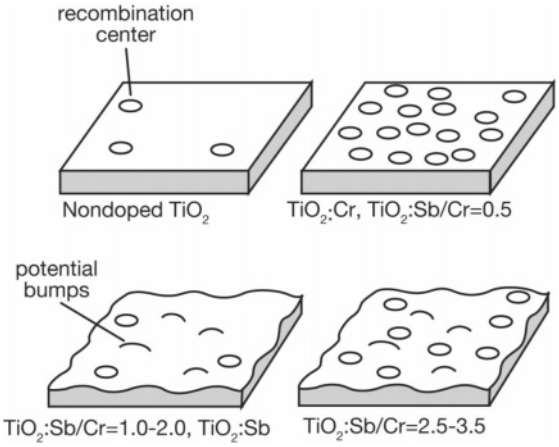

Figure 10. Interpretation of different recombination rates for non-doped TiO_2, TiO_2:Cr, TiO_2:Sb, and TiO_2:Sb/Cr photocatalysts. Note that the illustrations represent trapping and recombination in the bulk, not on the surface.

dopants were disproportionate to Sb^{3+} and Sb^{5+}.[13] When Sb^{3+} and Sb^{5+} dopants are compensated in the rutile lattice, electrons and holes are merely trapped and released as in TiO_2:Sb/Cr = 1.0.

By doping more Sb, the recombination rate was increased. The first-order time constant decreased to 330 μs for TiO_2:Sb/Cr = 2.5 and 170 μs for TiO_2:Sb/Cr = 3.5. Antimony trivalent cations of 0.076 nm radius[36] are definitely larger than the other cations, Ti^{4+}, Cr^{3+}, and Sb^{5+}. The TiO_2 lattice is deformed when substituted by the large Sb^{3+} cations. Recombination centers are created in TiO_2:Sb/Cr = 3.5 containing 2.3 mol % Cr with 5.8 mol % Sb in the starting material. The absolute absorbance at the time delay = 0 was smaller by half on TiO_2:Sb/Cr = 3.0 than on the other catalysts. This relationship suggests that the recombination probability in a nanosecond domain is positively related to the probability in the microsecond domain, as was found with differently prepared pristine TiO_2 catalysts.[19]

The recombination kinetics were insensitive to the pump light wavelengths. Decay curves observed with 532-nm pulses are presented in panel b of Figure 9. With 355-nm irradiation, electrons are excited to the conduction band with holes in the valence band. With 532-nm irradiation, electrons are still excited to the conduction band and holes are created in the Cr^{3+}-derived occupied states in the band gap. The recombination kinetics were insensitive to what states the holes were created in. This is probably because holes created in the valence band transferred to the Cr^{3+}-derived states. The occupied states of Cr^{3+} are proposed to give the donor band in TiO_2:Sb/Cr catalysts on the basis of photoluminescence results.[13] Holes migrate in the donor band until recombined. Electrons in the conduction band are thought to be more mobile than the holes in the valence and donor bands. Thus, the recombination rate is determined by the frequency of holes visiting recombination centers.

The four panels of Figure 10 illustrate our interpretation of the observed dynamics in the catalyst bulk. The non-doped TiO_2 calcined at 1420 K provides a highly periodic lattice including a limited number of recombination centers. When a photoexcited hole arrives at a center, it recombines with one of the mobile electrons. Excess Cr dopants cause additional recombination centers, oxygen vacancies, and Cr^{6+} cations. The population of the recombination centers should be in the order of dopant concentration, 10^{-2} per Ti atom. This number is high and the recombination is completed within 50 ns in TiO_2:Cr and TiO_2:Sb/Cr = 0.5. When Cr^{3+} dopants are compensated with the equivalent number of Sb^{5+}, Cr^{6+} cations and oxygen vacancies are removed. The TiO_2 lattice is perturbed just enough to trap the charge carriers. The rate of recombination is reduced compared with the non-doped TiO_2 because of the less mobile charge carriers visiting the original number of recombination centers. When TiO_2:Cr is doped with too much Sb, the lattice is deformed to produce a moderate number of recombination centers. The rate of recombination is accordingly enhanced.

In addition to the recombination centers in the bulk, which were illustrated in the panels, centers at the catalyst surface contribute partially. Antimony is more volatile than chromium, and the surface of the calcined catalysts can be Cr-rich. When Cr dopants are incompletely compensated at the surface, dopant-induced recombination centers are produced. Photoexcited carriers migrating from the bulk are recombined at the surface with incompletely compensated dopants. This is a possible reason for the restricted O_2 production observed for TiO_2:Sb/Cr = 1.0.

Charge compensation of the cationic dopants is essential in this scheme of sensitization. Electrons and holes are trapped on compensated dopants without much enhancing recombination. It is an open question how the compensated dopants do this. Theoretical simulations show promise to make clear the full nature of the dopant-derived states describing energetic and spatial distributions. Successful applications of simulations have already been demonstrated on nitrogen-doped[37] and carbon-doped[38] TiO_2.

Doping Cr and Sb even with the optimum ratio did not enhance the O_2 production when compared with the undoped TiO_2. With a steady-state UV light irradiation (wavelength > 300 nm) the production rate was 357 μmol h^{-1} on TiO_2, 45 μmol h^{-1} on TiO_2:Sb/Cr = 2.4, and none on TiO_2:Cr.[13] The rate of the surface reaction is related to a number of reasons. The number of excited charge carriers in the catalyst bulk, which was traced in our IR absorption, the carrier transport from the bulk to the surface, and the reaction probability at the surface can contribute equally to the steady-state reaction rate. The reduced rate of recombination does not necessarily provide an enhanced reaction rate. The trap-and-release transport proposed on TiO_2:Sb/Cr possibly reduces the UV-derived rate of O_2 production. The presence of Sb codopants enhanced the O_2 production remarkably compared with TiO_2:Cr. This is the subject of the present study.

It is important to experimentally determine the lateral distribution of the compensated dopants in the rutile lattice. The appropriate number ratio of the two dopants may guarantee compensation with random distribution. On the other hand, Cr^{3+} and Sb^{5+} paired in a definite local arrangement may be substituted for Ti^{4+} pairs. When the latter is the case, the paired dopants are recognized as an inorganic chromophore embedded in TiO_2. The resonance enhancement of the B_{2g} Raman bands suggests good symmetry around each Cr dopant atom. This provides negative evidence of the paired Cr−O−Sb dopants. A more direct determination of the local structure may be possible with extended X-ray absorption fine structure.

4. Conclusions

(1) Rutile particles doped with Cr and Sb were active for photocatalytic O_2 production from an $AgNO_3$ solution. A Sb/Cr ratio of more than unity was required to drive the photocatalytic reaction under visible (λ > 420 nm) light irradiation.

(2) On the sensitized catalysts, two vibrational modes of 700 and 810 cm^{-1} appeared in Raman scattering resonant to the electronic absorption. They are assigned to coupled, symmetric breathing modes of each CrO_6 octahedron and neighboring TiO_6

octahedra. The vibrational coupling suggests Cr dopant atoms exactly replaced Ti cations in the rutile lattice. The ability of resonance Raman scattering to know the local structure of sensitized light absorption centers is demonstrated.

(3) Electrons excited with 355-nm and 532-nm light pulses presented a monotonous absorption of mid-IR light. Electron−hole recombination in rutile was retarded by doping with Sb/Cr = 1−2. We propose that electrons and holes are merely trapped on the dopants without much enhancing recombination. The recombination was enhanced significantly with excess Cr dopants and enhanced moderately with excess Sb dopants.

(4) The optimized Sb/Cr ratios were common for visible light-induced O_2 production and for retarded recombination. This suggests that the charge carriers of the retarded recombination drive the surface reaction.

Acknowledgment. This work was supported by the Core Research for Evolutional Science and Technology (CREST) Program of the Japan Science and Technology Agency (JST).

References and Notes

(1) Domen, K.; Kondo, J. N.; Hara, M.; Takata, T. *Bull. Chem. Soc. Jpn.* **2000**, *73*, 1307.
(2) Kato, H.; Kudo, A. *Catal. Today* **2003**, *78*, 561.
(3) Kudo, A. *Catal. Surv. Asia* **2003**, *7*, 31.
(4) Kudo, A.; Kato, H.; Tsuji, I. *Chem. Lett.* **2004**, 1534.
(5) Abe, R.; Takata, T.; Sugihara, H.; Domen, K. *Chem. Commun.* **2005**, 3829.
(6) Kato, H.; Hori, M.; Konta, R.; Shimodaira, Y.; Kudo, A. *Chem. Lett.* **2004**, *33*, 1348.
(7) Maeda, K.; Domen, K. *J. Phys. Chem. C* **2007**, *111*, 7851.
(8) Sayama, K.; Nomura, A.; Arai, T.; Sugita, T.; Abe, R.; Yanagida, M.; Oi, T.; Iwasaki, Y.; Abe, Y.; Sugihara, H. *J. Phys. Chem. B* **2006**, *110*, 11352.
(9) Paola, A. D.; Marcì, G.; Palmisano, L.; Schiavello, M.; Uosaki, K.; Ikeda, S.; Ohtani, B. *J. Phys. Chem. B* **2002**, *106*, 637.
(10) Herrmann, J.-M.; Disdier, J.; Pichat, P. *Chem. Phys. Lett.* **1998**, *108*, 618.
(11) Palmisano, L.; Auguglio, V.; Sclafani, A.; Schiavello, M. *J. Phys. Chem.* **1988**, *92*, 6710.
(12) Serpone, N.; Lawless, D. *Langmuir* **1994**, *10*, 643.
(13) Kato, H.; Kudo, A. *J. Phys. Chem. B* **2002**, *106*, 5029.
(14) Yamakata, A.; Ishibashi, T.; Onishi, H. *J. Mol. Catal. A* **2003**, *199*, 85.
(15) Yamakata, A.; Ishibashi, T.; Takeshita, K.; Onishi, H. *Top. Catal.* **2005**, *35*, 211.
(16) Szczepankiewicz, S. H.; Moss, J. A.; Hoffmann, M. R. *J. Phys. Chem. B* **2002**, *106*, 2922.
(17) Chen, T.; Zhaochi, Z.; Wu, G.; Shi, J.; Ma, G.; Ying, P.; Li, C. *J. Phys. Chem. C* **2007**, *111*, 8005.
(18) Thompson, T. L.; Yates, J. T. J. *Chem. Rev.* **2006**, *106*, 4428.
(19) Yamakata, A.; Ishibashi, T.; Onishi, H. *Chem. Phys.* **2007**, *339*, 133.
(20) Yamakata, A.; Ishibashi, T.; Onishi, H. *J. Phys. Chem. B* **2001**, *105*, 7258.
(21) Yamakata, A.; Ishibashi, T.; Onishi, H. *Chem. Phys. Lett.* **2001**, *333*, 271.
(22) Takeshita, K.; Yamakata, A.; Ishibashi, T.; Onishi, H.; Nishijima, K.; Ohno, T. *J. Photochem. Photobiol., A* **2006**, *177*, 269.
(23) Takeshita, K.; Sasaki, Y.; Kobashi, M.; Tanaka, Y.; Maeda, S.; Yamakata, A.; Ishibashi, T.; Onishi, H. *J. Phys. Chem. B* **2003**, *107*, 4156.
(24) Ikeda, T.; Fujiyoshi, S.; Kato, H.; Kudo, A.; Onishi, H. *J. Phys. Chem. B* **2006**, *110*, 7883.
(25) Yamakata, A.; Ishibashi, T.; Kato; Kudo; Onishi, H. *J. Phys. Chem. B* **2003**, *107*, 14383.
(26) Porto, S. P. S.; Fleury, P. A.; Damen, T. C. *Phys. Rev.* **1967**, *154*, 522.
(27) Mestl, G.; Ruiz, P.; Delmon, B.; Knözinger, H. *J. Phys. Chem. B* **1994**, *98*, 11276.
(28) Moujin, J.; Bihan, T. L.; Lucazeau, G. *J. Phys. Chem. Solids* **2001**, 553.
(29) National Institute of Advanced Industrial Science and Technology. *Raman Spectra Database of Minerals and Inorganic Materials (RASMIN)*, 2007; ASMIN Web: http://www.aist.go.jp/RIODB/rasmin/E_index.html.
(30) Iliev, M. N.; Litvinchuk, A. P.; Lee, H.-G.; Chu, C. W.; Barry, A.; Coey, J. M. D. *Phys. Rev. B* **1999**, *60*, 33.
(31) Albrecht, A. C. *J. Chem. Phys.* **1961**, *34*, 1476.
(32) Zhang, J.; Li, M.; Feng, Z.; Chen, J.; Li, C. *J. Phys. Chem. B* **2006**, *110*, 927.
(33) Skinner, D. E.; Colombo, D. P., J.; Cavaleri, J. J.; Bowman, R. M. *J. Phys. Chem.* **1995**, *99*, 7853.
(34) Pankove, J. I. *Optical Processes in Semiconductors*; Dover: New York, 1975.
(35) Katoh, R.; Furube, A.; Hara, K.; Murata, S.; Sugihara, H.; Arakawa, H.; Tachiya, M. *J. Phys. Chem. B* **2003**, *107*, 14383.
(36) Shannon, R. D. *Acta Crystallogr., Sect. A* **1976**, *32*, 751.
(37) Livraghi, S.; Paganini, M. C.; Giamello, E.; Selloni, A.; Di Valentin, C.; Pacchioni, G. *J. Am. Chem. Soc.* **2006**, *128*, 15666.
(38) Di Valentin, C.; Pacchioni, G.; Selloni, A. *Chem. Mater.* **2005**, *17*, 6656.